Submitted to
32nd International Conference on High Energy Physics, ICHEP04, August 16, 2004, Beijing
Abstract: **5-0163**
Parallel Session **5**
www-h1.desy.de/h1/www/publications/conf/conf_list.html

Inclusive $D^{*\pm}$ Meson and Associated Dijet Production in Deep-Inelastic Scattering

H1 Collaboration

Abstract

The inclusive production of $D^{*\pm}$ mesons in deep inelastic scattering is studied with the H1 detector at HERA using an integrated luminosity of 47.0 pb^{-1}. In the kinematic region $2 \leq Q^2 \leq 100$ GeV^2 and $0.05 \leq y \leq 0.7$ an e^+p cross section for inclusive $D^{*\pm}$ meson production of $7.72 \pm 0.23\,(\mathrm{stat.}) \pm 1.09\,(\mathrm{syst.})\,\mathrm{nb}$ is measured in the visible range $1.5 \leq p_{t,D^*} \leq 15$ GeV and $|\eta_{D^*}| \leq 1.5$. Single and double differential inclusive $D^{*\pm}$ meson cross sections are compared to perturbative calculations in the framework of the DGLAP and CCFM evolution schemes. The additional requirement is then made that there are at least two jets with $E_{t,\text{ jet 1}} \geq 4$ GeV, $E_{t,\text{ jet 2}} \geq 3$ GeV in the Breit frame of reference and $-1 \leq \eta_{\text{lab, jet 1,2}} \leq 2.5$. In this kinematic range the inclusive cross section for dijet production associated with a $D^{*\pm}$ meson is found to be $1.63 \pm 0.10\,(\mathrm{stat.}) \pm 0.25\,(\mathrm{syst.})\,\mathrm{nb}$. Differential cross sections for dijet events with $D^{*\pm}$ mesons are also presented and compared to QCD model predictions. Models which provide a good description of inclusive $D^{*\pm}$ production are found to provide a poorer description of jet production with $D^{*\pm}$ mesons.

1 Introduction

Results on $D^{*\pm}$ meson production in deep inelastic scattering (DIS) have been published by the H1 and ZEUS collaborations [1–5]. The analysis described in this paper uses the data collected during the 1999 and 2000 running periods with positrons at HERA, yielding a significantly larger integrated luminosity of 47.0 pb^{-1} than used in the previous publications [1, 3, 5]. As a result, the $D^{*\pm}$ production cross section is measured with increased precision, and the measurement of two jet production in events with at least one tagged $D^{*\pm}$ meson becomes possible in DIS.

The description of open heavy flavour production in deep-inelastic ep collisions is based on perturbative QCD with the assumption that Q^2 and the heavy quark mass provide the necessary hard scale. To leading order (LO), photon gluon fusion ($\gamma g \rightarrow Q\bar{Q}$) is the dominant production process. The experimental results on inclusive $D^{*\pm}$ meson production are compared with predictions made using two different pQCD approaches with the charm quarks considered to be massive: a next-to-leading order (NLO) calculation [6–8] based on collinear factorisation and the DGLAP evolution equations [9] and another calculation based on k_t factorisation and parton evolution according to the CCFM equations [10]. In both approaches, gluons and light quarks are assumed to be the only active flavours in the proton and therefore charm is produced perturbatively only via photon gluon fusion. The CCFM approach is expected to provide a better description of gluon evolution at very low values of Bjorken-x.

Following the same line as in a previous publication [5] the HVQDIS program by Harris and Smith [11] has been used to perform comparisons of the data with the NLO DGLAP scheme and with the hadron level Monte Carlo generator CASCADE [12] which implements the CCFM scheme.

2 Detector and Data Sample

The data presented were collected with the H1 detector at HERA during the running periods of 1999 and 2000. In that period HERA operated with 27.5 GeV positrons and 920 GeV protons colliding at a center-of-mass energy of $\sqrt{s} = 318$ GeV. The data amount to an integrated luminosity of $\mathcal{L} = 47.0$ pb^{-1}. A detailed description of the H1 detector [17], [18] and the components that are most relevant for this analysis is given in [5].

3 Event Selection and Kinematics

The identification and selection of the scattered positron is performed as described in [5].

The geometrical acceptance cuts for the backward calorimeter (SpaCal) and the backward drift chamber (BDC) impose a limitation on the measured positron scattering angle of $\theta_e < 178^\circ$. In order to ensure high acceptance for the entire kinematic region, the square of the four momentum transfer is restricted to $2 \leq Q^2 \leq 100$ GeV^2 and the inelasticity to $0.05 \leq y \leq 0.7$.

At fixed center-of-mass energy $\sqrt{s}$, the kinematics of the inclusive scattering process $ep \to eX$ can be completely determined by using any two of the independent Lorentz variables: the Bjorken scaling variables x and y, the four momentum squared of the virtual photon and the invariant mass squared W^2 of the hadronic final state. In this analysis, these variables are determined from the measurement of the energy E'_e and the polar angle θ_e of the scattered positron according to

$$\begin{aligned} Q^2 &= 4E_e E'_e \cos^2\left(\frac{\theta_e}{2}\right) & y &= 1 - \frac{E'_e}{E_e}\sin^2\left(\frac{\theta_e}{2}\right) \\ x &= \frac{Q^2}{ys} & W^2 &= Q^2\left(\frac{1-x}{x}\right) \end{aligned} \tag{1}$$

where E_e, is the electron beam energy.

First a fully reconstructed $D^{*\pm}$ meson in the visible range of the detector is required. D^{*+} mesons are reconstructed using the decay chain $D^{*+} \longrightarrow D^0\pi_s^+ \longrightarrow K^-\pi^+\pi_s^+$. The method applied is described in detail in [1, 5].

The range of the transverse momentum and the pseudorapidity of the $D^{*\pm}$ meson is restricted to $1.5 \leq p_{t,D^*} \leq 15$ GeV and $|\eta_{D^*}| \leq 1.5$ where η is defined as $\eta = -\ln\tan\left(\frac{\theta}{2}\right)$. These cuts are applied in order to ensure that the events lie in a region of the detector where the acceptance is high and well understood. The distribution of the mass difference $\Delta m = m_{K\pi\pi} - m_{K\pi}$ is shown in figure 1. A total of 2604 ± 77 $D^{*\pm}$ mesons is obtained.

Figure 2 shows the energy and polar angle distributions of the scattered positron for events with an identified $D^{*\pm}$ meson. The data are compared to the prediction of the RAPGAP Monte Carlo. The RAPGAP [19] Monte Carlo allows the non-diffractive as well as the diffractive DIS events to be simulated. Here it is used to simulate the production of charm via the BGF process. Good agreement is observed between the data and the simulation.

In order to define the jet sample within the events containing a $D^{*\pm}$ meson candidate, the k_t-cluster algorithm [20] in its inclusive mode is used in the Breit frame. The hadronic final state is reconstructed from all energy depositions in the SpaCal and the liquid argon calorimeter as well as from the track momenta measured in the tracking system. When applying the jet algorithm the momenta of the three particles originating from the reconstructed $D^{*\pm}$ meson are treated as one particle with the four-vector of the tagged $D^{*\pm}$ meson. The E recombination scheme (in which the four-vectors of the objects are added) is used.

The transverse energy of the leading jet in the Breit frame is required to be $E_{t,\text{ jet 1}} \geq 4$ GeV, the transverse energy of the second jet $E_{t,\text{ jet 2}} \geq 3$ GeV and the pseudorapidities of the two leading jets in the laboratory frame $-1 \leq \eta_{\text{jets}} \leq 2.5$. A total of 836 ± 51 events fulfill the jet requirements.

4 Inclusive $D^{*\pm}$ Meson Cross Sections

The cross section for $D^{*\pm}$ meson production in deep inelastic ep scattering is calculated from the observed number of $D^{*\pm}$ candidates, $N_{D^{*\pm}}$, according to

$$\sigma(e^+p \to e^+D^{*\pm}X) = \frac{N_{D^{*\pm}}}{\mathcal{L} \cdot Br \cdot \epsilon \cdot (1+\delta_{\text{rad}})}. \quad (2)$$

Here, $\mathcal{L}$ and Br refer to the integrated luminosity and the branching ratio $Br(D^{*+} \to D^0\pi^+) \cdot Br(D^0 \to K^-\pi^+) = 0.0259$ [21]. The efficiency ϵ is estimated using the RAPGAP Monte Carlo program [19]. The radiative corrections are obtained using HERACLES.

The inclusive cross section for $D^{*\pm}$ meson production in the kinematic region $2 \leq Q^2 \leq 100$ GeV^2, $0.05 \leq y \leq 0.7$ and in the visible D^{*+} range $1.5 \leq p_{t,D^*} \leq 15$ GeV and $|\eta_{D^*}| \leq 1.5$ is found to be

$$\sigma_{vis}(e^+p \to e^+D^{*\pm}X) = 7.72 \pm 0.23(\text{stat.}) \ \pm 1.09\,(\text{syst.})\ \text{nb}.$$

The errors refer to the statistical and systematic error, respectively. The largest contribution to the systematic error is due to the uncertainty in the track reconstruction efficiency. Other important sources of systematic error include the uncertainty in the determination of the background shape in the Δm distribution, the D^0 mass resolution and the uncertainty introduced by the difference in the acceptance and efficiency corrections obtained by making use of the RAPGAP and HERWIG Monte Carlos.

The visible inclusive $D^{*\pm}$ meson production cross section was calculated in the NLO DGLAP scheme with the HVQDIS program using the CTEQ5F3 proton parton densities [22]. The predictions range from 4.90 nb for a charm quark mass $m_c = 1.5$ GeV and Peterson fragmentation parameter $\epsilon_c = 0.10$ to 6.62 nb for $m_c = 1.3$ GeV and $\epsilon_c = 0.035$. The hadronization fraction $f(c \to D^{*+}) = 0.233 \pm 0.010 \pm 0.011$ [23] was used. For the same variation of m_c and ϵ_c, calculations based on the CCFM evolution equation, as implemented in the CASCADE program, yield cross sections of 6.79 nb and 8.82 nb, respectively. The measured value of the cross section agrees better with the CASCADE prediction than with that from HVQDIS.

In figure 3 the inclusive single differential $D^{*\pm}$ cross sections in the visible region are shown as a function of the event variables W, x and Q^2 and as a function of the $D^{*\pm}$ observables p_t, η and the inelasticity $z_{D^*} = P \cdot p_{D^*}/P \cdot q = (E-p_z)_{D^*}/2yE_e$, where P, q and p_{D^*} denote the four-momenta of the incoming proton, the exchanged photon and the observed $D^{*\pm}$ meson, respectively.

Fig. 3 also includes the expectations from the HVQDIS program using the CTEQ5F3 parton density. The charm quark mass and the fragmentation parameter have been varied from $m_c = 1.3$ GeV and $\epsilon_c = 0.035$ to $m_c = 1.5$ GeV and $\epsilon_c = 0.10$. The dark shaded band indicates the uncertainties in the predictions due to these variations. Although the predicted visible cross section is smaller than that experimentally observed, there is reasonable agreement with the data in the shapes of the different single differential cross sections with the exception of the region $\eta > 0$, where the measured $D^{*\pm}$ meson production cross section is larger than that predicted. Since in the boson gluon fusion process the forward region ($\eta > 0$) is correlated with small z_{D^*}, a similar discrepancy between data and theory is observed at small z_{D^*}.

The predictions of the CASCADE program, with the same variations of the charm quark mass and fragmentation parameter, are also presented in Fig. 3. The expectations from the

CASCADE program are found to agree better with the data, particularly in the positive η region. Similar conclusions were drawn in [5] based on a sample of significantly smaller luminosity.

In Fig. 4 the cross section is compared with the expectations of the RAPGAP Monte Carlo when only direct processes are taken into account, and when the contribution of resolved processes is also considered. The comparison shows that the prediction of RAPGAP with direct processes only lies slightly below the observed cross section and that taking into account the resolved contribution does not result in a good description of the data, the prediction then often being too high.

In order to enable the study of correlations among the observables in $D^{*\pm}$ meson production, Figs. 5, 6, 7 and 8 show the double differential inclusive $D^{*\pm}$ cross sections. It is evident that the excess observed in the data with respect to the HVQDIS expectation at large pseudorapidities ($0.5 < \eta_{D^*} < 1.5$) is independent of Q^2 and is concentrated at small $p_{t\,D^*}$ and small z_{D^*}.

5 Associated Dijet Cross Sections

The cross section for dijet production associated with a $D^{*\pm}$ meson in deep inelastic ep collisions is obtained from the number of dijet events fulfilling the dijet criteria which include at least one $D^{*\pm}$ candidate in a manner similar to that described for the inclusive $D^{*\pm}$ meson cross section measurement.

The inclusive cross section for dijet and $D^{*\pm}$ meson production in the kinematic region $2 \leq Q^2 \leq 100$ GeV^2, $0.05 \leq y \leq 0.7$, $1.5 \leq p_{t,D^*} \leq 15$ GeV and $|\eta_{D^*}| \leq 1.5$ with jets with Breit frame transverse energies $E_{t,\text{ jet 1}} \geq 4$ GeV, $E_{t,\text{ jet 2}} \geq 3$ GeV and laboratory pseudorapidities $-1 \leq \eta_{\text{jet 1,2}} \leq 2.5$ is found to be

$$\sigma_{vis}(e^+p \to e^+D^{*\pm}\text{dijet}\,X) = 1.63 \pm 0.10\,(\text{stat.}) \pm 0.25\,(\text{syst.})\ \text{nb}.$$

In addition to the systematic errors which arise in the measurement of the $D^{*\pm}$ meson cross sections, additional systematic effects contribute in this measurement. The most important additional errors arise from the uncertainty of the energy measurement in the main and backward calorimeters and the dependence of the acceptance calculation on the Monte Carlo models used.

The purity and the stability of the sample is above 40 % in all bins.

In figure 9 the differential $D^{*\pm}$ meson dijet cross sections are presented as a function of the event variables Q^2, x, the maximum transverse jet energy $E_t^{\text{max}} = E_{t,\text{ jet 1}}$, and the rapidity difference of the dijets, $\Delta\eta = |\eta_{\text{jet 1}} - \eta_{\text{jet 2}}|$, the latter two being measured in the Breit frame. The data are compared with the expectations from CASCADE and RAPGAP for direct and the sum of direct and resolved processes. Here, for both Monte Carlo predictions, the values $m_c = 1.4$ GeV and $\epsilon_c = 0.078$ were used for the charm quark mass and the fragmentation parameter, respectively. In CASCADE the initial gluon distribution is fitted to the inclusive F_2 data, while the CTEQ5L proton parton density is used in the RAPGAP Monte Carlo.

It can be seen that RAPGAP predictions for direct processes are below the measured cross sections particularly for small Bjorken-x, large E_t^{max} and small $\Delta\eta$.

In figure 10 the cross section for the production of dijets with an associated $D^{*\pm}$ meson is shown versus the $D^{*\pm}$ meson production cross section and is compared with the expectation of the RAPGAP, AROMA [24], HERWIG and CASCADE Monte Carlo generators. The models, even those that provide a good description of the inclusive $D^{*\pm}$ meson cross section, do not describe the measured associated dijet cross section in events with a $D^{*\pm}$ meson.

6 Conclusions

New measurements of differential cross sections for inclusive $D^{*\pm}$ production in deep inelastic ep scattering are presented. The data are compared with predictions based on both NLO DGLAP and CCFM formalisms, using the HVQDIS program and the CASCADE model, respectively. The expectations of the CCFM based model provide a better description of the inclusive $D^{*\pm}$ data, especially in the positive pseudorapidity region.

A measurement of the cross section for the production of dijets and an associated $D^{*\pm}$ meson in DIS is performed and is compared to Monte Carlo predictions. The RAPGAP Monte Carlo describes the Q^2 and x dependence of the cross section only when both direct and resolved contributions are taken into account, lying below the data when only direct processes are considered. Measurements of the differential cross sections for associated dijet and $D^{*\pm}$ meson production are presented and compared with the RAPGAP and CASCADE expectations. Even though the inclusive $D^{*\pm}$ meson production cross section is described reasonably well by RAPGAP and is in good agreement with the expectation using the CCFM based model CASCADE, the associated dijet cross section is found to be less well described by both models.

References

[1] C. Adloff *et al.* [H1 Collaboration], Z. Phys. C **72** (1996) 593 [hep-ex/9607012].

[2] J. Breitweg *et al.* [ZEUS Collaboration], Phys. Lett. B **407** (1997) 402 [hep-ex/9706009].

[3] C. Adloff *et al.* [H1 Collaboration], Nucl. Phys. B **545** (1999) 21.

[4] J.Breitweg et al. [ZEUS Collaboration], Eur. Phys. J. C12 (2000) 1, 35-52.

[5] C. Adloff et al. [H1 Collaboration], Phys. Lett. B528 (2002) 199.

[6] E. Laenen, S. Riemersma, J. Smith and W. L. van Neerven, Phys. Lett. B **291** (1992) 325.

[7] E. Laenen, S. Riemersma, J. Smith and W. L. van Neerven, Nucl. Phys. B **392** (1993) 162; E. Laenen, S. Riemersma, J. Smith and W. L. van Neerven, Nucl. Phys. B **392** (1993) 229; S. Riemersma, J. Smith and W. L. van Neerven, Phys. Lett. B **347** (1995) 143 [hep-ph/9411431].

[8] B. W. Harris and J. Smith, Nucl. Phys. B **452** (1995) 109 [hep-ph/9503484]; B. W. Harris and J. Smith, Phys. Lett. B **353** (1995) 535 [Erratum-ibid. B **359** (1995) 423] [hep-ph/9502312].

[9] V. N. Gribov and L. N. Lipatov, Yad. Fiz. **15** (1972) 781 [Sov. J. Nucl. Phys. **15** (1972) 438]; V. N. Gribov and L. N. Lipatov, Yad. Fiz. **15** (1972) 1218 [Sov. J. Nucl. Phys. **15** (1972) 675]; L. N. Lipatov, Sov. J. Nucl. Phys. **20** (1975) 94 [Yad. Fiz. **20** (1975) 181]; G. Altarelli and G. Parisi, Nucl. Phys. B **126** (1977) 298; Y. L. Dokshitzer, Sov. Phys. JETP **46** (1977) 641 [Zh. Eksp. Teor. Fiz. **73** (1977) 1216].

[10] M. Ciafaloni, Nucl. Phys. B **296** (1988) 49; S. Catani, F. Fiorani and G. Marchesini, Phys. Lett. B **234** (1990) 339; S. Catani, F. Fiorani and G. Marchesini, Nucl. Phys. B **336** (1990) 18; G. Marchesini, Nucl. Phys. B **445** (1995) 49 [hep-ph/9412327].

[11] B. W. Harris and J. Smith, Phys. Rev. D **57** (1998) 2806 [hep-ph/9706334].

[12] H. Jung and G. P. Salam, Eur. Phys. J. C **19** (2001) 351 [hep-ph/0012143]; H. Jung, Comp. Phys. Proc. Comm. **143** (2002) 111 [hep-ph/0109102].

[13] T. Ahmed et al. [H1 Collaboration], Phys. Lett. B **297** (1992) 205; M. Derrick et al. [ZEUS Collaboration], Phys. Lett. B **297** (1992) 404; I. Abt et al. [H1 Collaboration], Phys. Lett. B **314** (1993) 436; M. Derrick et al. [ZEUS Collaboration], Phys. Lett. B **322** (1994) 287; J.Breitweg et al. [ZEUS Collaboration], Eur. Phys. J. C4 (1998) 591; C. Adloff et al. [H1 Collaboration], Eur. Phys. J. C1 (1998) 97; J.Breitweg et al. [ZEUS Collaboration], Eur. Phys. J. C11 (1999) 35; J.Breitweg et al. [ZEUS Collaboration], Eur. Phys. J. C1 (1998) 109.

[14] M. Derrick et al. [ZEUS Collaboration], Phys. Lett. B **342** (1995) 417; M. Derrick et al. [ZEUS Collaboration], Phys. Lett. B **348** (1995) 665.

[15] W. Bartel et al. [JADE Collaboration], Z. Phys. C **24** (1984); M. Althoff et al. [TASSO Collaboration], Z. Phys. C **31** (1986); C. Berger et al. [PLUTO Collaboration], Nucl. Phys. B **281** (1987); H. Aihara et al. [TPC/2M. Acciarri et al. [L3 Collaboration], Phys. Lett. B **436** (1998); R. Barate et al. [ALEPH Coll.], Comp. Phys. Comm. B **458** (1999); M. Acciarri et al. [L3 Collaboration], Phys. Lett. B **447** (1999); M. Acciarri et al. [L3 Collaboration], Phys. Lett. B **453** (1999).

[16] J.Breitweg et al. [ZEUS Collaboration], Phys. Lett. B **479** (2000) 39; C. Adloff et al. [H1 Collaboration], Phys. Lett. B **415** (1997) 418; C. Adloff et al. [H1 Collaboration], Eur. Phys. J. C13 (2000) 397; M. Acciarri et al. [L3 Collaboration], Phys. Lett. B **483** (2000).

[17] I. Abt et al. [H1 Collaboration], Nucl. Instrum. Meth. A386 (1997) 310.

[18] I. Abt et al. [H1 Collaboration], Nucl. Instrum. Meth. A386 (1997) 348.

[19] H.Jung, Comput. Phys. Commun. **86** (1995) 147.

[20] S. Catani et al, Nucl. Phys. B **406** (1993) 187; S.D. Ellis and D.E.Sopoer, Phys. Rev. D **48** (1993) 3160.

[21] K. Hagiwara et al., Phys. Rev. D **66** (2002) 010001.

[22] H.L.Lai, J.Fuston, S.Kuhlmann, J.Morfin, F.Olness, J.F.Owens, J.Pumplin, W.K.Tung Eur. Phys. J. C12 (2000) 375.

[23] R. Barate *et al.* [ALEPH Collaboration], Eur. Phys. J. C **16** (2000) 597 [hep-ex/9909032].

[24] G. Ingelman, J. Rathsman and G. A. Schuler, Comput. Phys. Commun. **101** (1997) 135 [hep-ph/9605285].

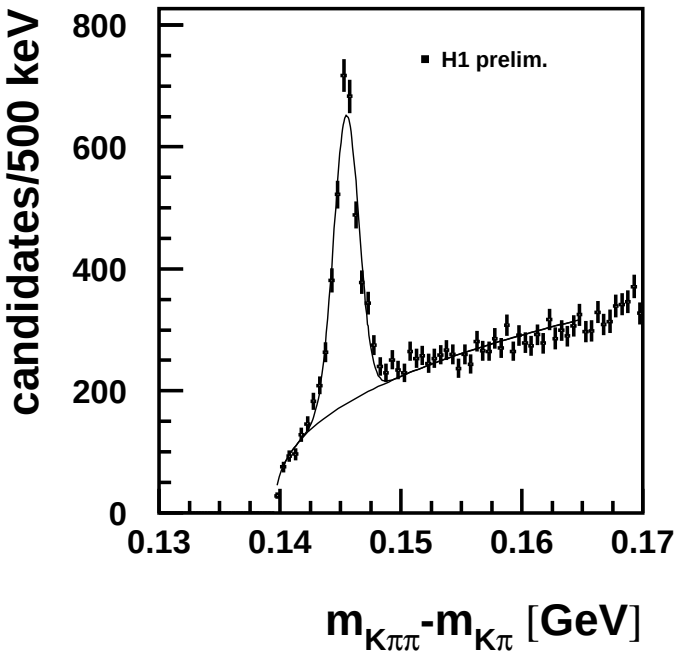

Figure 1: Distribution of the mass difference $\Delta m = m(K^{\mp}\pi^{\pm}\pi_s^{\pm}) - m(K^{\mp}\pi^{\pm})$ for DIS events in the visible range $1.5 \leq p_t \leq 15$ GeV and $|\eta| \leq 1.5$. The curves represent a fit to the $m(K^{\mp}\pi^{\pm}\pi_s^{\pm})$ distribution using a Gaussian for the signal and a term $(\Delta m - m_{\pi})^{\alpha}$ for the background.

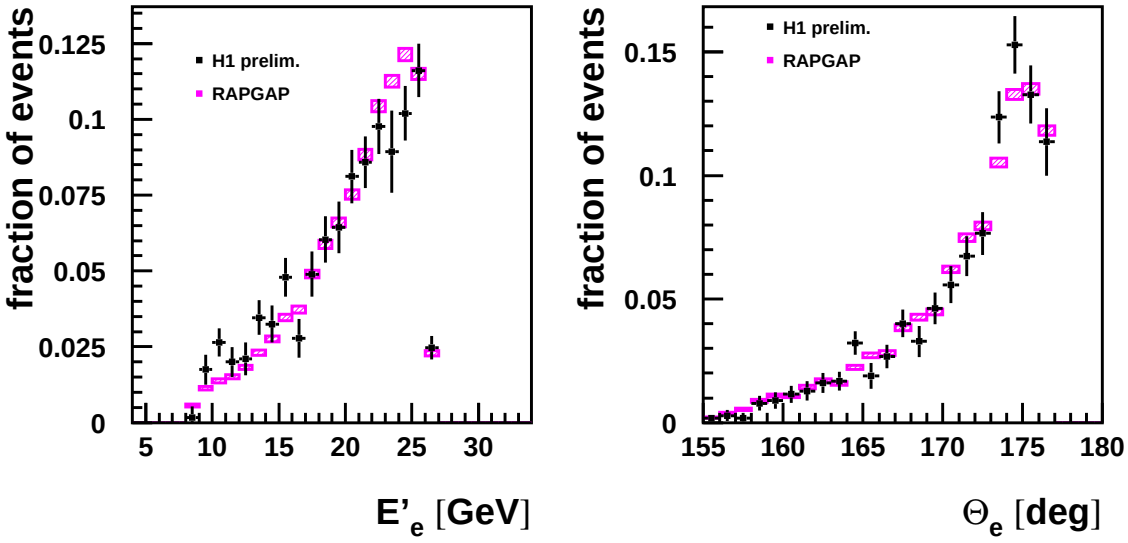

Figure 2: The reconstructed E'_e and θ_e for events with $D^{*\pm}$ candidates (after background subtraction) together with the detector level (RAPGAP) prediction (shaded histogram).

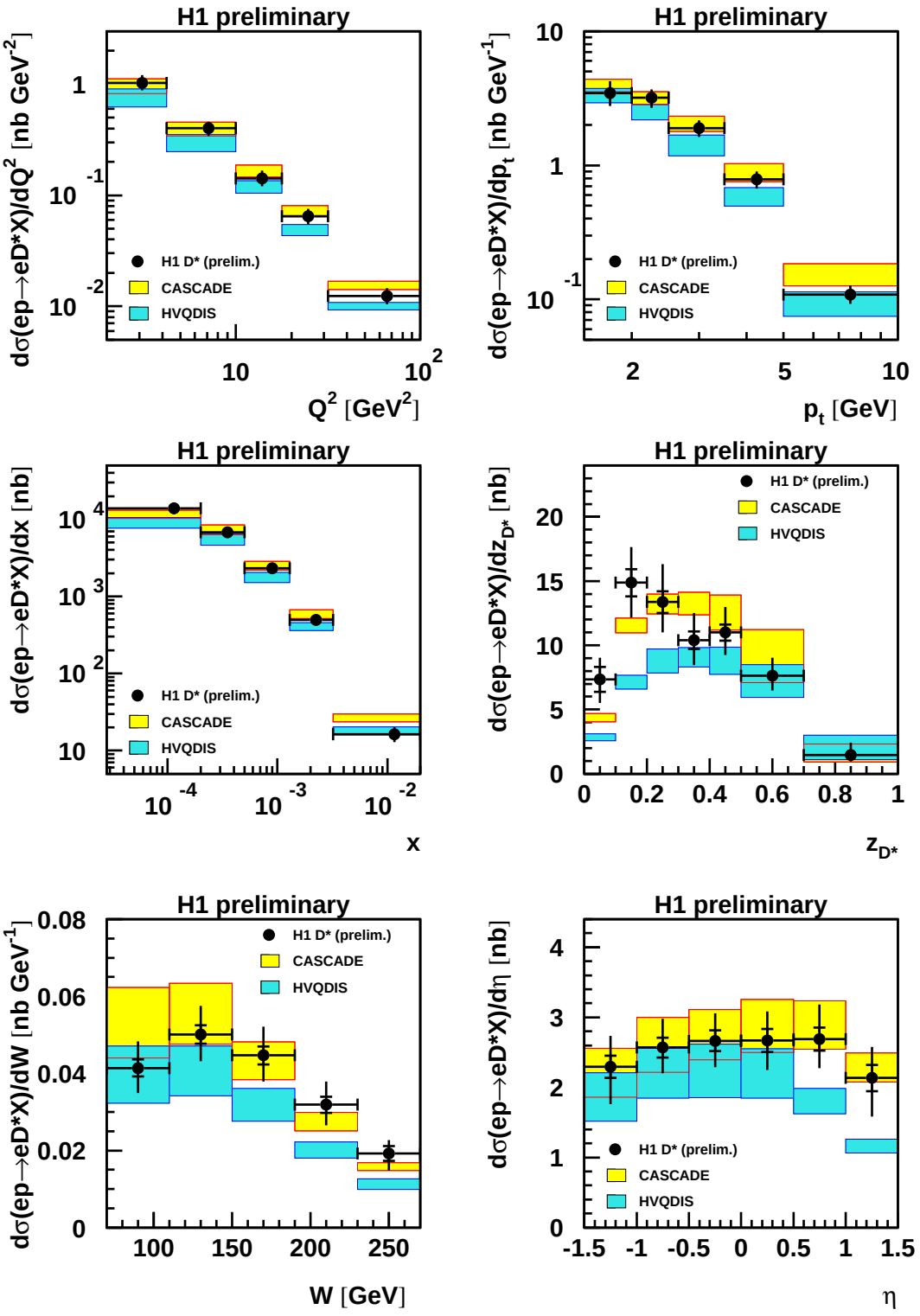

Figure 3: Single differential inclusive cross section for $D^{*\pm}$ meson production $\sigma(ep \to eD^{*\pm}X)$ versus W, x, Q^2, p_t, η and z_{D^*}. The inner and outer error bars correspond to the statistical and total errors. The expectation of the NLO DGLAP calculation using HVQDIS with CTEQ5F3 parton densities is indicated by the lower shaded band. The upper shaded band is the expectation of the CCFM calculations based on the CASCADE program with the initial gluon distribution fitted to the inclusive F_2 data. The upper and lower bounds of both calculations correspond to ($m_c = 1.3$ GeV, $\epsilon_c = 0.035$) and ($m_c = 1.5$ GeV, $\epsilon_c = 0.10$), respectively.

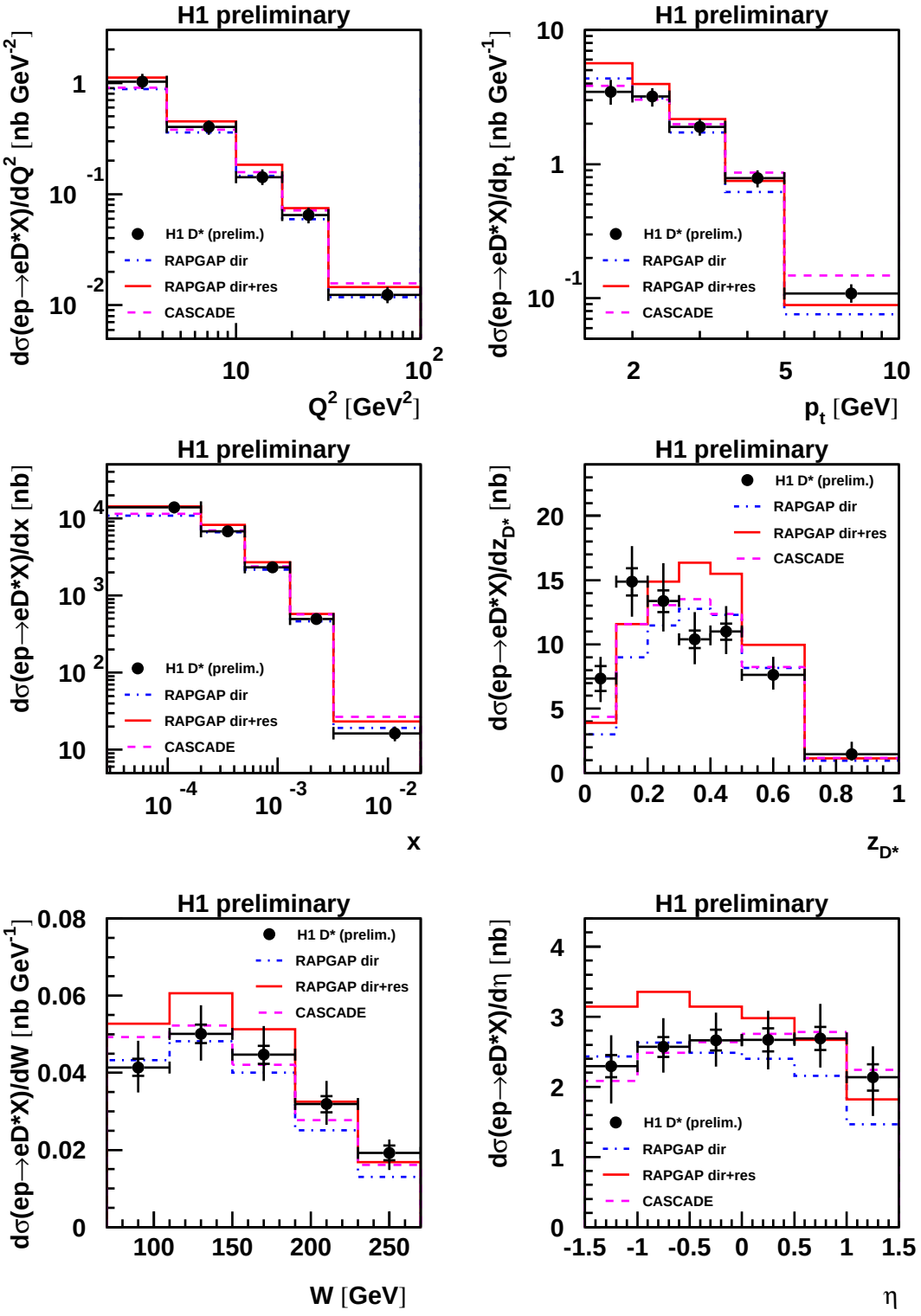

Figure 4: Single differential inclusive cross section for $D^{*\pm}$ meson production $\sigma(ep \to eD^{*\pm}X)$ versus W, x, Q^2, p_t, η and z_{D^*}. The inner and outer error bars correspond to the statistical and total errors. The expectation of the RAPGAP Monte Carlo (with $m_c = 1.4$ GeV, $\epsilon_c = 0.078$ and using the CTEQ5L proton parton densities) is shown when only direct processes are taken into account and when the resolved contribution is also considered. The expectation of the CASCADE program (with $m_c = 1.4$ GeV, $\epsilon_c = 0.078$ and the initial gluon distribution fitted to the inclusive F_2 data) is also displayed.

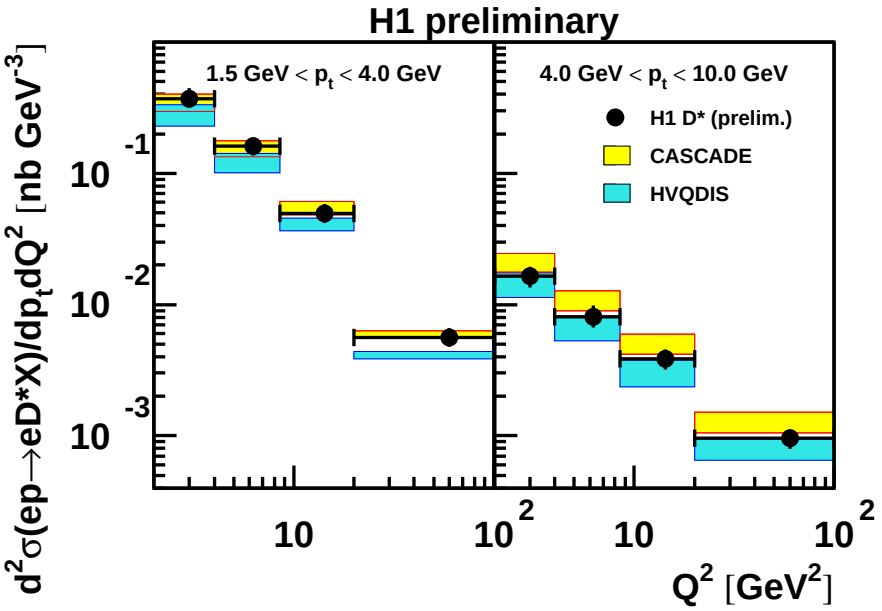

Figure 5: The double differential inclusive cross section for $D^{*\pm}$ meson production $\mathrm{d}^2\sigma/\mathrm{d}p_t\mathrm{d}Q^2$ in bins of p_t. The inner and outer error bars correspond to the statistical and total errors. The expectations of the NLO DGLAP calculation using HVQDIS and of the CCFM calculations based on the CASCADE program are also indicated (see figure 3 for details).

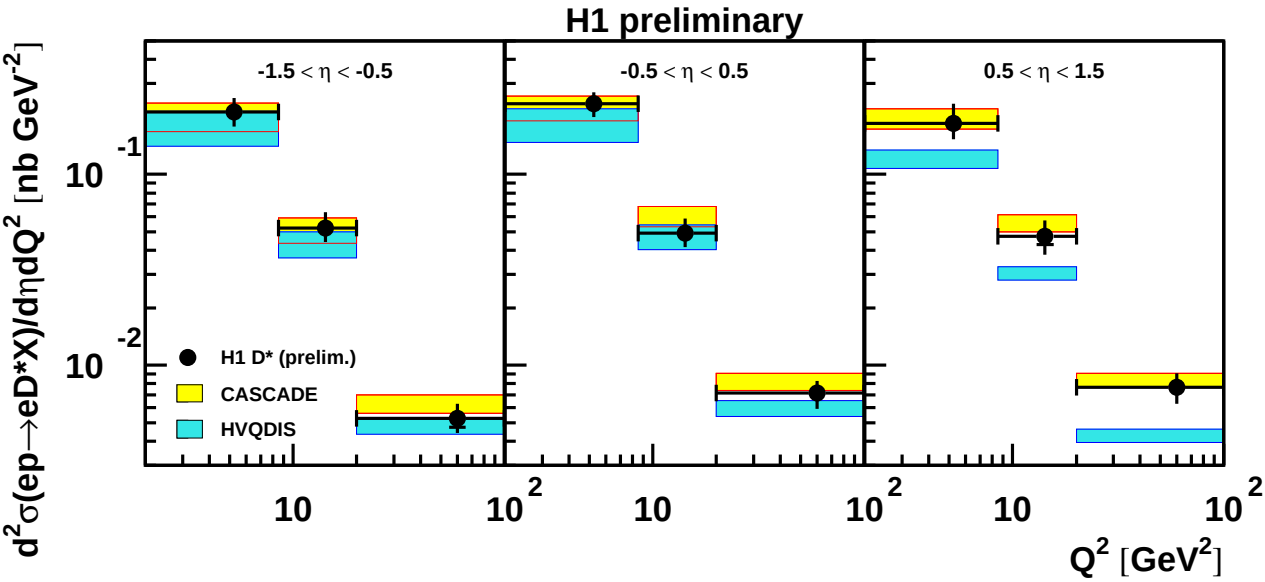

Figure 6: The double differential inclusive cross section for $D^{*\pm}$ meson production $\mathrm{d}^2\sigma/\mathrm{d}\eta\mathrm{d}Q^2$ in bins of η. The inner and outer error bars correspond to the statistical and total errors. The data are compared to the expectations of the NLO DGLAP calculation using HVQDIS and of the CCFM calculations based on the CASCADE program (see figure 3 for details).

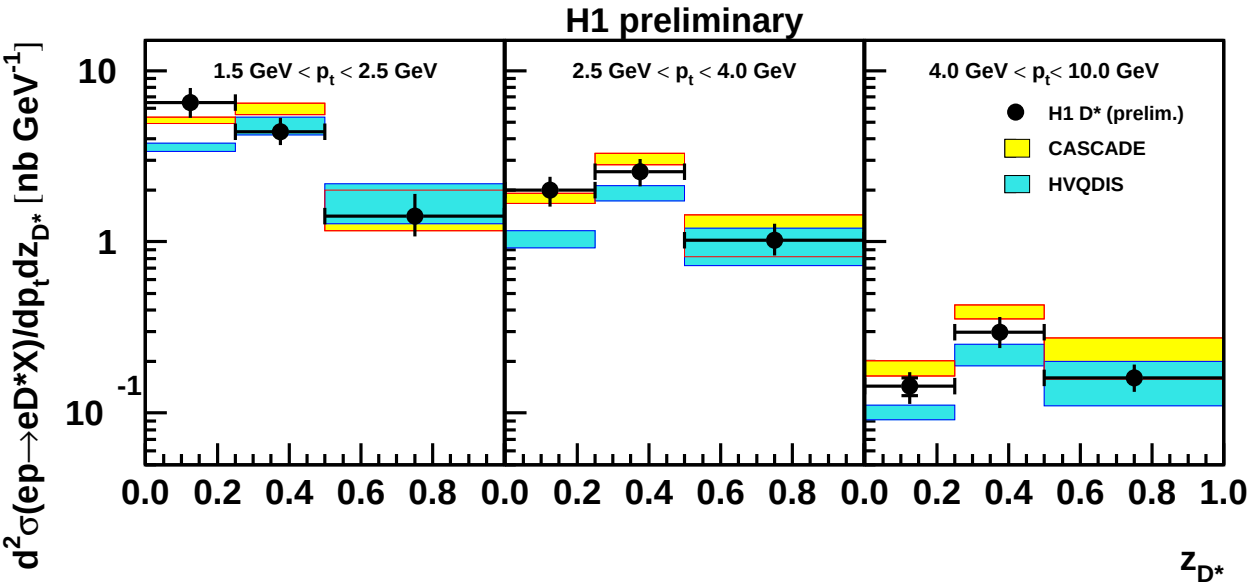

Figure 7: Double differential inclusive cross section for $D^{*\pm}$ meson production $\mathrm{d}^2\sigma/\mathrm{d}p_t\mathrm{d}z_{D^*}$ in bins of p_t. The inner and outer error bars correspond to the statistical and total errors. The data are compared to the expectations of the NLO DGLAP calculation using HVQDIS and of the CCFM calculations based on the CASCADE program (see figure 3 for details).

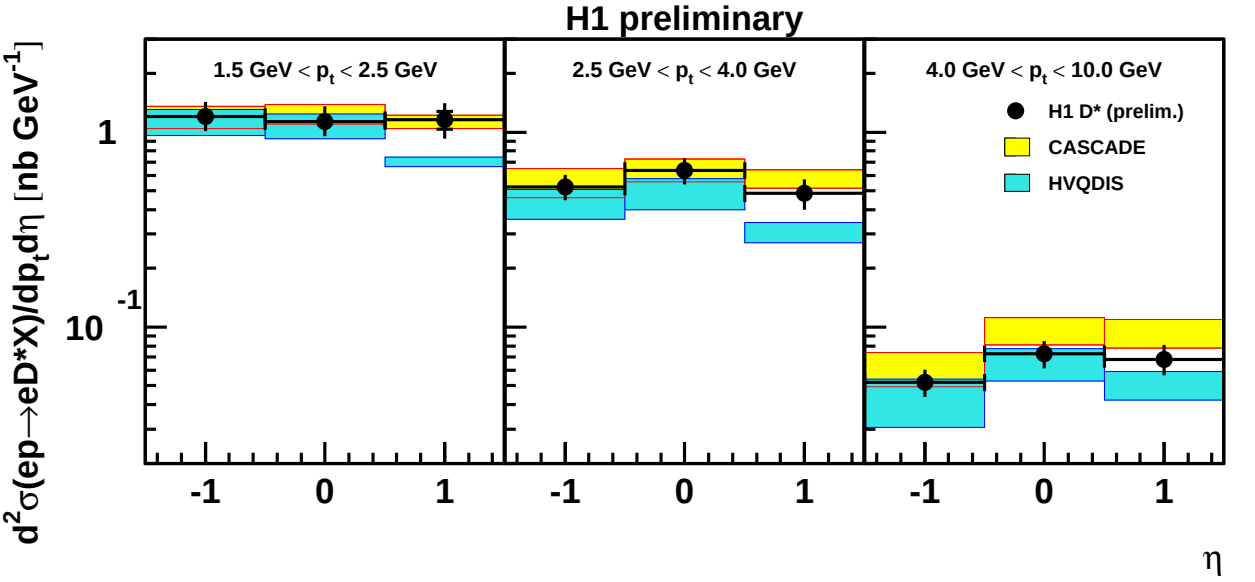

Figure 8: Double differential inclusive cross section for $D^{*\pm}$ meson production $\mathrm{d}^2\sigma/\mathrm{d}p_t\mathrm{d}\eta$ in bins of p_t. The inner and outer error bars correspond to the statistical and total errors. The data are compared to the expectations of the NLO DGLAP calculation using HVQDIS and of the CCFM calculations based on the CASCADE program (see figure 3 for details).

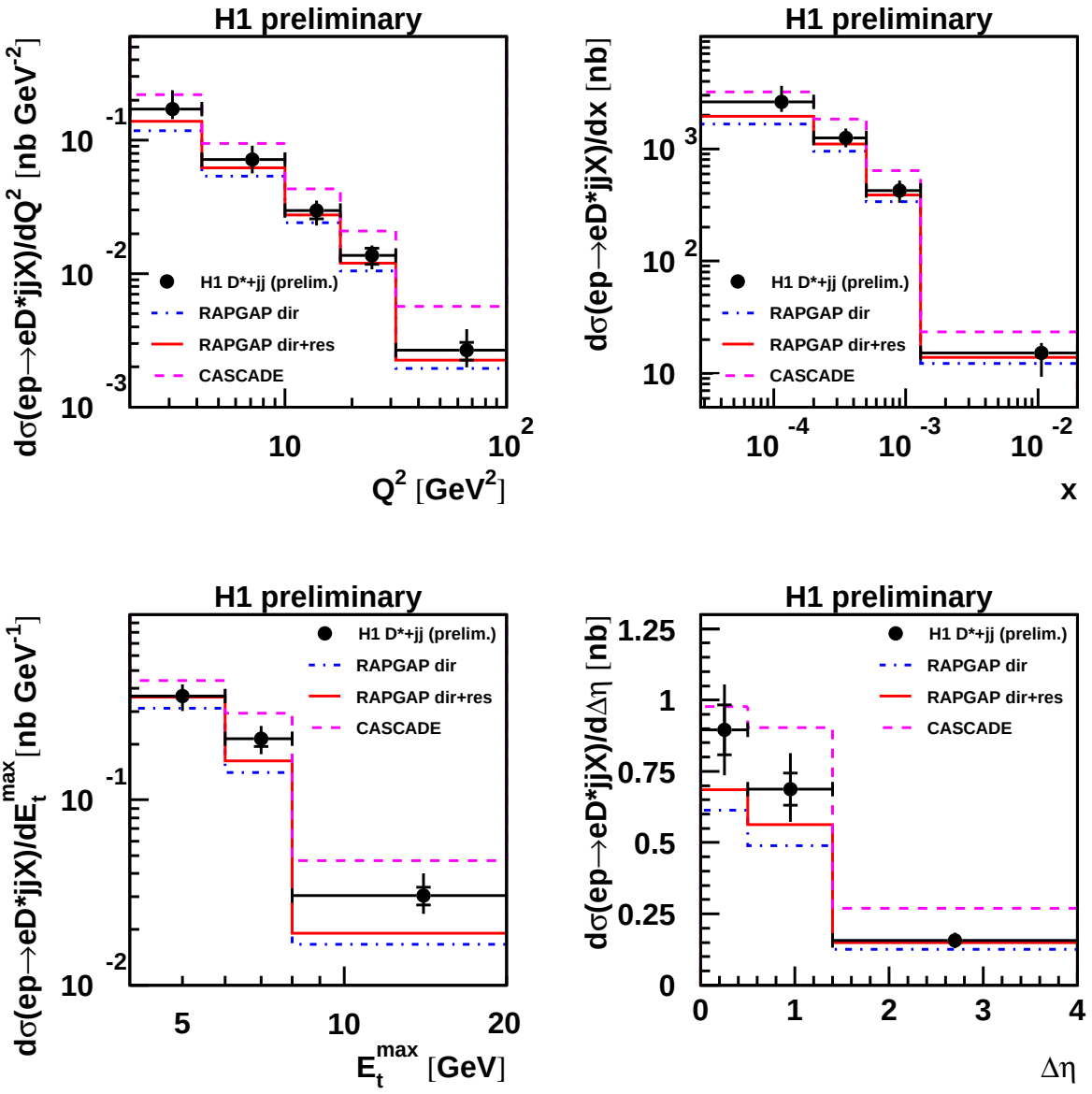

Figure 9: Dijet cross sections as a function of Q^2, x, $E_t^{\rm max}$ and $\Delta\eta$, the latter two being measured in the Breit frame, for events with $D^{*\pm}$ mesons. The inner and outer error bars correspond to the statistical and total errors. The expectation of the RAPGAP Monte Carlo (with $m_c = 1.4$ GeV, $\epsilon_c = 0.078$ and using the CTEQ5L parton density in the proton) is shown when only direct processes are taken into account and when the resolved contribution is also considered. The data are also compared with the expectation of the CASCADE Monte Carlo with $m_c = 1.4$ GeV, $\epsilon_c = 0.078$ and the initial gluon distribution fitted to the inclusive F_2 data.

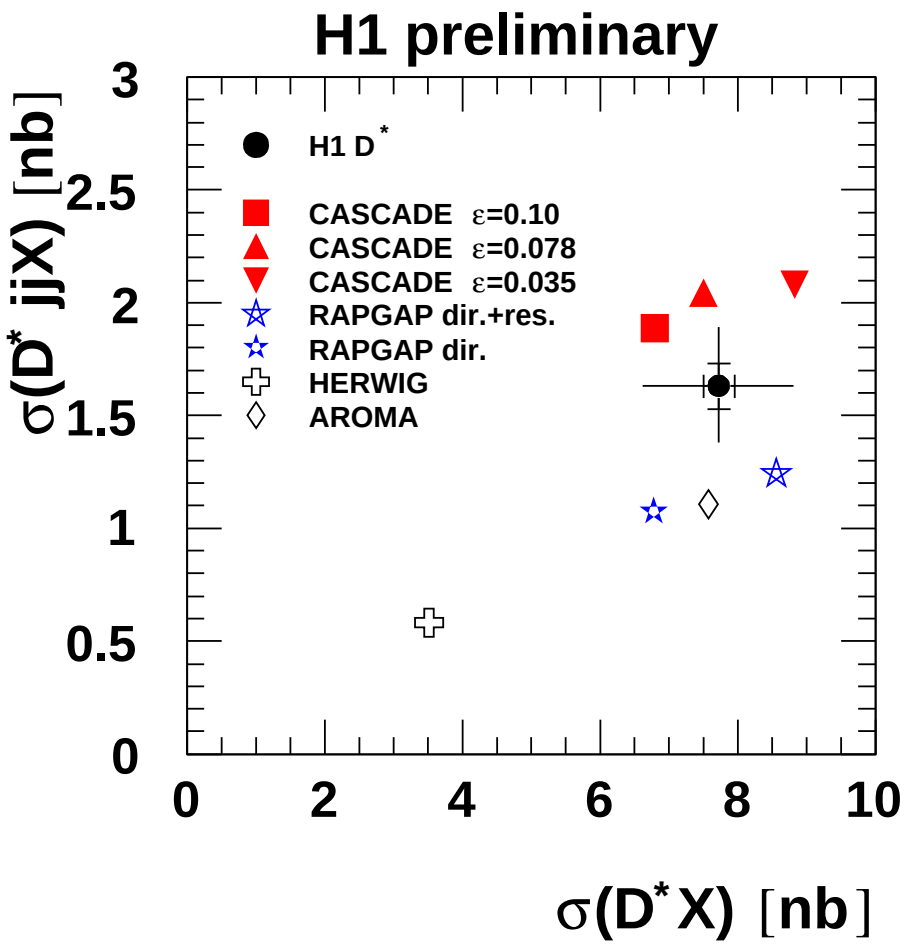

Figure 10: The cross section for the production of dijets in association with a $D^{*\pm}$ meson versus the $D^{*\pm}$ meson production cross section. The expectation of the RAPGAP Monte Carlo with $\epsilon_c = 0.078$ is shown when only direct processes are taken into account and when the resolved contribution is also considered. The predictions of the AROMA Monte Carlo with $\epsilon_c = 0.078$ and of the HERWIG Monte Carlo which uses cluster fragmentation are also displayed. For the predictions of RAPGAP, AROMA and HERWIG $m_c = 1.4$ GeV and the CTEQ5L proton parton densities are used. The data are also compared with the expectation of the CASCADE Monte Carlo with the initial gluon distribution fitted to the inclusive F_2 data, for $m_c = 1.4$ GeV, $\epsilon_c = 0.078$ for $m_c = 1.3$ GeV, $\epsilon_c = 0.035$ and for $m_c = 1.5$ GeV, $\epsilon_c = 0.10$.